Trends in mica–mica adhesion reflect the influence of molecular details on long-range dispersion forces underlying aggregation and coalignment

Dongsheng Li[a,1], Jaehun Chun[a,1], Dongdong Xiao[a], Weijiang Zhou[b], Huacheng Cai[c], Lei Zhang[b], Kevin M. Rosso[a], Christopher J. Mundy[a,d], Gregory K. Schenter[a], and James J. De Yoreo[a,e]

[a]Physical and Computational Sciences Directorate, Pacific Northwest National Laboratory, Richland, WA 99352; [b]Department of Applied Physics, School of Science, Xi'an Jiaotong University, Xi'an, Shaanxi 710049, China; [c]Department of Physics, University of Illinois at Urbana–Champaign, Urbana, IL 61801; [d]Department of Chemical Engineering, University of Washington, Seattle, WA 98195; and [e]Department of Materials Science and Engineering, University of Washington, Seattle, WA 98195

Edited by Patricia M. Dove, Virginia Tech, Blacksburg, VA, and approved June 8, 2017 (received for review December 22, 2016)

Oriented attachment of nanocrystalline subunits is recognized as a common crystallization pathway that is closely related to formation of nanoparticle superlattices, mesocrystals, and other kinetically stabilized structures. Approaching particles have been observed to rotate to achieve coalignment while separated by nanometer-scale solvent layers. Little is known about the forces that drive coalignment, particularly in this "solvent-separated" regime. To obtain a mechanistic understanding of this process, we used atomic-force-microscopy-based dynamic force spectroscopy with tips fabricated from oriented mica to measure the adhesion forces between mica (001) surfaces in electrolyte solutions as a function of orientation, temperature, electrolyte type, and electrolyte concentration. The results reveal an ∼60° periodicity as well as a complex dependence on electrolyte concentration and temperature. A continuum model that considers the competition between electrostatic repulsion and van der Waals attraction, augmented by microscopic details that include surface separation, water structure, ion hydration, and charge regulation at the interface, qualitatively reproduces the observed trends and implies that dispersion forces are responsible for establishing coalignment in the solvent-separated state.

orientation-dependent interparticle forces | dynamic force spectroscopy | atomic force microscopy | solvent structure | DLVO theory

Crystallization by particle attachment (CPA) is a common mechanism by which single crystals form in solutions (1). In contrast to classical growth processes of monomer-by-monomer addition and Ostwald ripening, CPA occurs through assembly of higher-order species ranging from multi-ion complexes (2) and polymeric clusters (3) to fully formed nanocrystals. Among the numerous styles of CPA, none has garnered more attention than oriented attachment (OA) by which crystalline nanoparticles assemble into larger single-crystal structures through attachment on coaligned crystal faces (4, 5). OA often leads to formation of hierarchical structures, such as highly branched nanowires (6), tetrapods (7), and nanoparticle superlattices (8), endowed with unique properties (9) that are inexorably tied to this nonclassical process of crystallization.

OA has been inferred for metals (10), semiconductors (11), and insulating oxides (6); it has been directly observed via liquid phase transmission electron microscopy (LP-TEM) (5), and the evolution of particle distributions during OA has been captured with cryogenic TEM (12). OA is highly dependent on solution conditions, including pH, ionic strength, and temperature, and is marked by two important stages. In the first stage, particles approach one another but do not make contact; rather they remain separated by an intervening solvent layer of $O(1)$ nm in thickness (5). This solvent-separated state can occur on such an extensive scale that a kinetically stabilized particle array—sometimes referred to as a mesocrystal—is formed in which particles are crystallographically coaligned, but not in contact (12). In the second stage, the attachment barrier associated with the layer is overcome and particles fuse via a sudden "jump-to-contact" (5).

LP-TEM studies have led to estimates of the magnitude of the short-range attractive force that drives the second stage (5), but little is known about either the orientation dependence (13, 14) of the long-range forces that lead to alignment in the critical first stage or their variation as the intervening structured solvent layer, induced by the presence of the two crystal surfaces, evolves in response to particle approach. Of equal importance for understanding OA are the effects on these long-range forces from changes in solution conditions, including electrolyte concentrations and temperature, both of which should impact the structure of near-surface solvent layers and their ability to create energy minima that define solvent-separated states (15).

Near-surface solvent structure and interaction forces between surfaces (such as those of mica plates) have been investigated via atomic force microscopy (AFM) (16), surface force apparatus (SFA) (13, 17, 18), and theoretical modeling (19, 20). Those studies showed there are at least three minima in force vs. distance between two mica surfaces that exhibit a periodicity of about 3 Å corresponding to the approximate thickness of a water

Significance

Crystal growth through nanoparticle assembly appears to be a common phenomenon in synthetic, biological, and geochemical settings, and can lead to formation of hierarchical structures with unique properties tied to this nonclassical assembly process, but the underlying forces driving assembly are poorly understood. Using custom-made single-crystal atomic force microscopy tips, we measured the adhesion force between mica surfaces in the solvent-separate regime as a function of crystallographic orientation and solution parameters. The observed dependencies are predicted using a continuum description of the electrostatic and electrodynamic interactions that includes short-range molecular details. The findings show that the attractive interaction driving nanoparticle assembly and orientation results from the coupling between the short-range solution response and the long-range van der Waals interactions.

Author contributions: D.L., K.M.R., C.J.M., and J.J.D.Y. designed research; D.L. and D.X. performed experiments; D.L., J.C., W.Z., H.C., L.Z., K.M.R., C.J.M., and G.K.S. analyzed data; J.C., C.J.M., and G.K.S. developed the theory; W.Z., H.C., and L.Z. assisted with data processing; and D.L., J.C., C.J.M., G.K.S., and J.J.D.Y. wrote the paper.

The authors declare no conflict of interest.

This article is a PNAS Direct Submission.

Freely available online through the PNAS open access option.

[1]To whom correspondence may be addressed. Email: dongsheng.li2@pnnl.gov or Jaehun.Chun@pnnl.gov.

This article contains supporting information online at www.pnas.org/lookup/suppl/doi:10.1073/pnas.1621186114/-/DCSupplemental.

layer (21). Both X-ray reflectivity (21) and frequency-modulated AFM measurements (16) confirm this repeated layering above the mica surface. However, few studies have probed the long-range interactions that drive crystal coalignment in the solvent-separated state. Dynamic force spectroscopy (22) (DFS) measurements in aqueous solutions using a constant imposed force that produces varying but $\geq O(1)$-nm separations, depending on physicochemical parameters, provide the opportunity to probe these interactions and their orientation dependence in the solvent-separated regime, and understand the impact of such parameters on the interactions.

We performed DFS (22) using an AFM equipped with a rotation stage to directly probe the interaction forces between crystal facets as a function of in-plane orientation. During DFS, an AFM tip is brought toward a substrate where it adheres before being retracted at a rate R that is systematically varied. The resulting "spectrum" of adhesion forces F_{ad} probes two fundamental regimes (22): a near-equilibrium regime where entering and leaving the bound state occurs on a timescale comparable with the rate of tip retraction, and a kinetic regime where tip retraction is too rapid to allow for bound states to reform once dissociated. From an analysis of the F_{ad} vs. R, the equilibrium free energy of binding ΔG_b is determined (22).

We chose mica for this investigation, because fresh (001) planes are easily generated and extensive studies of mica–mica interactions have been performed using an SFA (13, 17), providing a basis for interpreting the current work. Moreover, unlike SFA (13), the flat-surface geometry and relatively small interacting surface area in DFS facilitates varying the relative orientation of tip and substrate through a full 360° rotation in a single experiment.

AFM tips were fabricated from single crystals of mica such that the lower surface of each tip presented an atomically flat (001) face (Fig. 1*A*). (See *Methods* for details.) A second mica crystal was used as the substrate against which the tip was brought until a maximum compressive force of 2–4 nN was reached. Further comparison with previous SFA measurements places the minimum tip–substrate separation at ~1 nm, which lies beyond the first and possibly the second hydration layers of the two surfaces (21). (See the discussion below and *SI Appendix* for a rationale to estimate the separation.)

Upon approach of the tip to the surface (red curve in Fig. 1*B*), force curves typically displayed a small jump-to-contact (circled region in Fig. 1*B*) before entering the repulsive regime and exhibited a much larger F_{ad} upon retraction (blue curve in Fig. 1*B*), as is typically seen, for example, with silicon and silicon nitride tips on mica (23). Measurements in NaCl solutions showed a strong dependence on concentration, but essentially no dependence on tip retraction rate (Fig. 1*C*). The lack of dependence on retraction rate implies the measurements were taken at near-equilibrium over the entire range of rates. This outcome is strikingly different from that observed for atomic and molecular bonds and has two consequences. First, the independence of F_{ad} from the retraction rate suggests that the nature of adhesion between mica surfaces is in a solvent-separated state that is distinct from that of molecular bonds probed in previous DFS measurements probing molecular bonds (22). Second, and most important from the standpoint of interpreting the data, the relative values of F_{ad} are a direct measure of the relative magnitudes of ΔG_b.

Taking advantage of the equilibrium nature of the force measurement, we quantified the effect of in-plane angular mismatch on mica–mica adhesion energy by measuring F_{ad} at a single retraction rate. Rotation of the mica substrate in deionized water led to a periodicity in F_{ad} with minima approximately every 60° over the full 360° of rotation and with the maxima exceeding the minima (F_{max}/F_{min}) by a factor of ~2 (Fig. 2). This result is consistent with previous SFA data (13) showing an orientation dependence of adhesion forces between two mica surfaces (limited to ±10° variation around the maximum), but extends the measurement to a full 360° of rotation. The observed minima also appeared as sharp cusps in this periodic pattern, although the minimum at 180° appeared to be considerably shallower than the others. For comparison, using the same tip to perform the measurement on an amorphous oxide layer on silicon produces no discernible periodicity and a variability of only ±13%.

We next investigated F_{ad} at 100 mM salt concentration for each electrolyte. Normalizing F_{ad} to the value in pure water, the results reveal a trend of decreasing adhesion-free energy from salt-free to divalent to monovalent ions, with F_{ad} in the presence of Mg^{2+} or Na^+ exceeding that for Ca^{2+} or K^+, respectively (Fig. 3*A*). In the case of Na^+, for which an extensive set of F_{ad} was collected (Fig. 4*A*), our results show F_{ad} falls rapidly as the NaCl concentration (C_{NaCl}) increases to about 10 mM, then rises to a secondary maximum between 20 and 30 mM, before falling gradually at higher concentrations. Finally, we examined the dependence of F_{ad} on temperature (T) for a range of C_{NaCl} (Fig. 3*B*). The results display a systematic trend of increasing F_{ad} with T, except at the highest C_{NaCl} (100 mM) for which F_{ad} first decreases with T before exhibiting the same trend as all other concentrations.

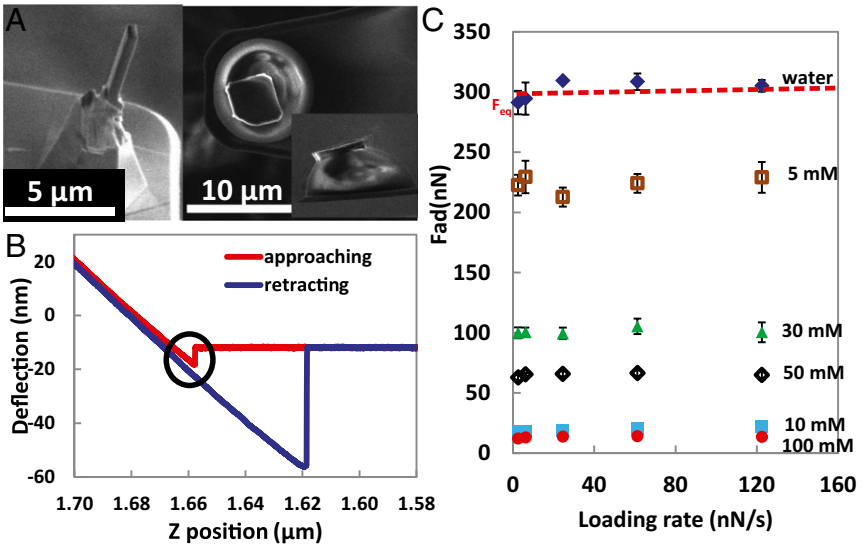

Fig. 1. Experimental approach to determining mica–mica adhesion energies. (*A*) SEM images of customized AFM probes with single-crystal mica tips presenting (001) faces. (*B*) Typical force curves in NaCl salt solution displaying a small jump (black circle) to the minimum tip–surface separation upon approach (red curve) and a large rupture force upon retraction (blue curve). (*C*) F_{ad} vs. loading rate (tip retraction rate) at various NaCl concentrations, showing no rate dependence.

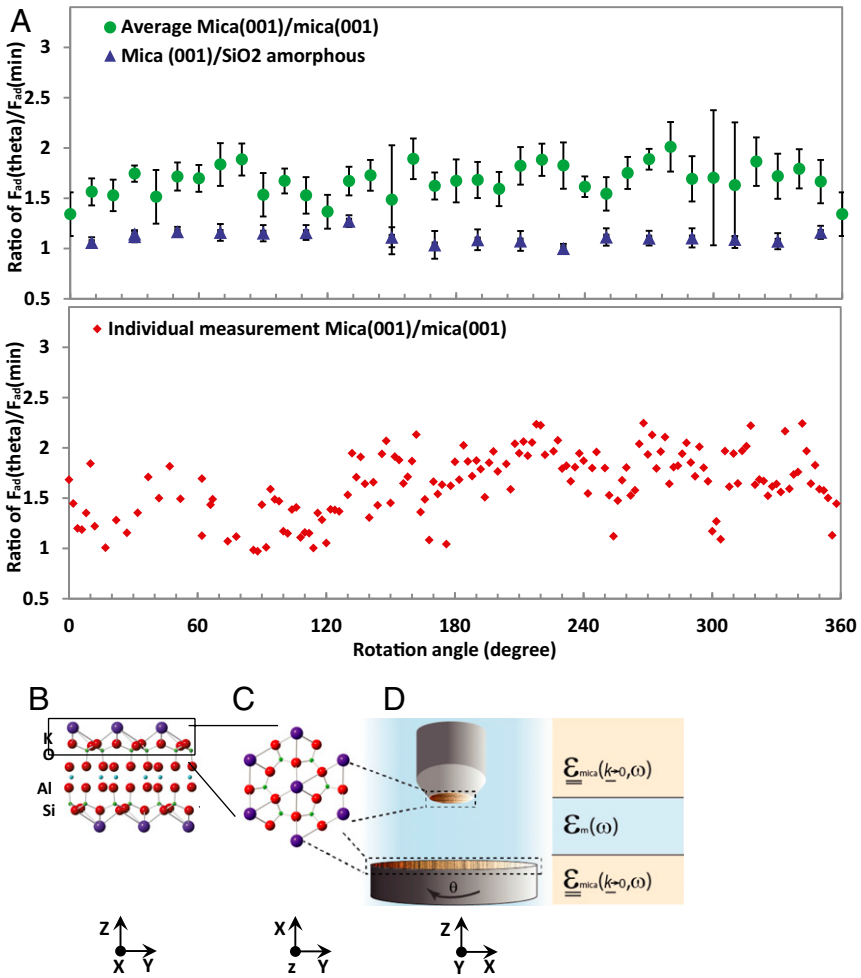

Fig. 2. Dependence of F_{ad} on relative in-plane orientation. (*A*) F_{ad} plotted as F_{max}/F_{min} vs. rotation angle for a mica (001) tip against a mica (001) face (red diamonds and green solid circles) and an amorphous SiO_2 surface (blue triangles). Rotation step between individual measurements (red diamonds) is 2° except between 20 and 100°, where it is 5 ± 1° due to instrumental limitations. Green solid circles are averages of data points taken within 10° intervals. For a number of the maxima, the data suggest a small minimum (i.e., at 40, 90, and 150°) near the peak; 0° is arbitrary. The error bar stands for 1 SD. F_{min} is taken from the individual data set for the F_{ad}(theta)/F_{ad}(min) plots of both the average and individual measurements. (*B* and *C*) Schematic showing monoclinic structure of mica as viewed along [010] and [001] directions, respectively. *(D)* Schematic of experimental setup highlighting the distinct values of the dielectric function, ϵ, in the three regions and its tensorial nature within the solid regions.

The observed dependence of F_{ad} on orientation shows that, even at substantial distances, the underlying symmetry of the crystal lattice impacts the intercrystal interactions, whereas the nonmonotonic dependence of F_{ad} on C_{NaCl} suggests multiple types of forces are competing. Moreover, the increase in F_{ad} with T implies that the conventional model of molecular bond rupture is not applicable to solvent-separated crystal–crystal contacts, because the former predicts a decreasing rupture force with

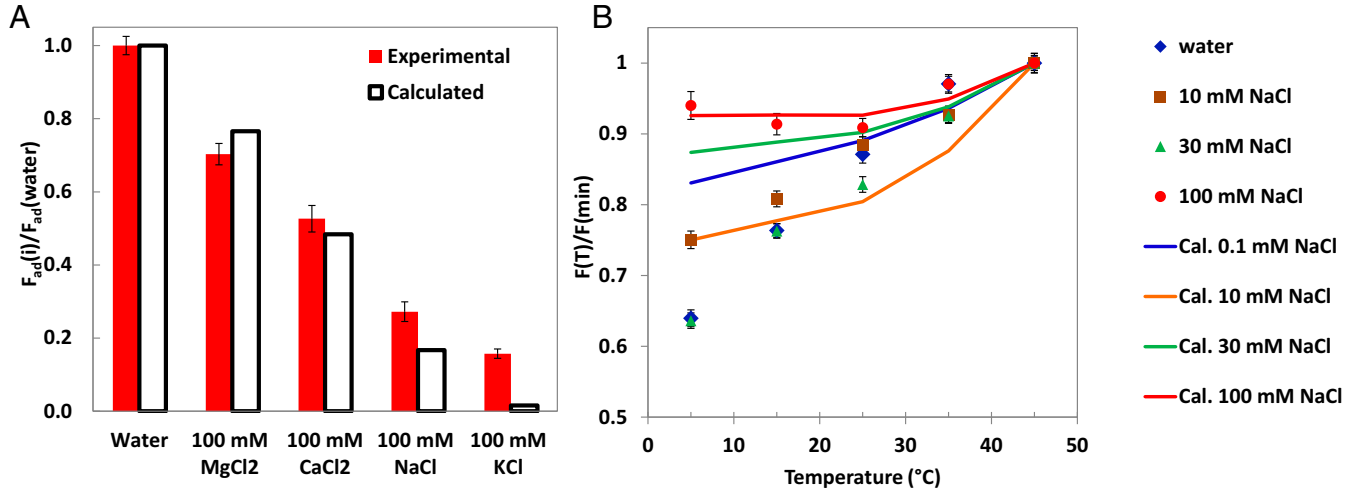

Fig. 3. Dependence of F_{ad} on electrolyte type and temperature (T). Experimental and calculated values of F_{ad} (*A*) for a range of electrolytes, where F_{ad} is normalized to that for pure water, and (*B*) vs. T for a range of C_{NaCl}, where F_{ad} is normalized to the value at 45 °C. The calculated curve for 0.1 mM NaCl was used for comparison with the observed values in pure water.

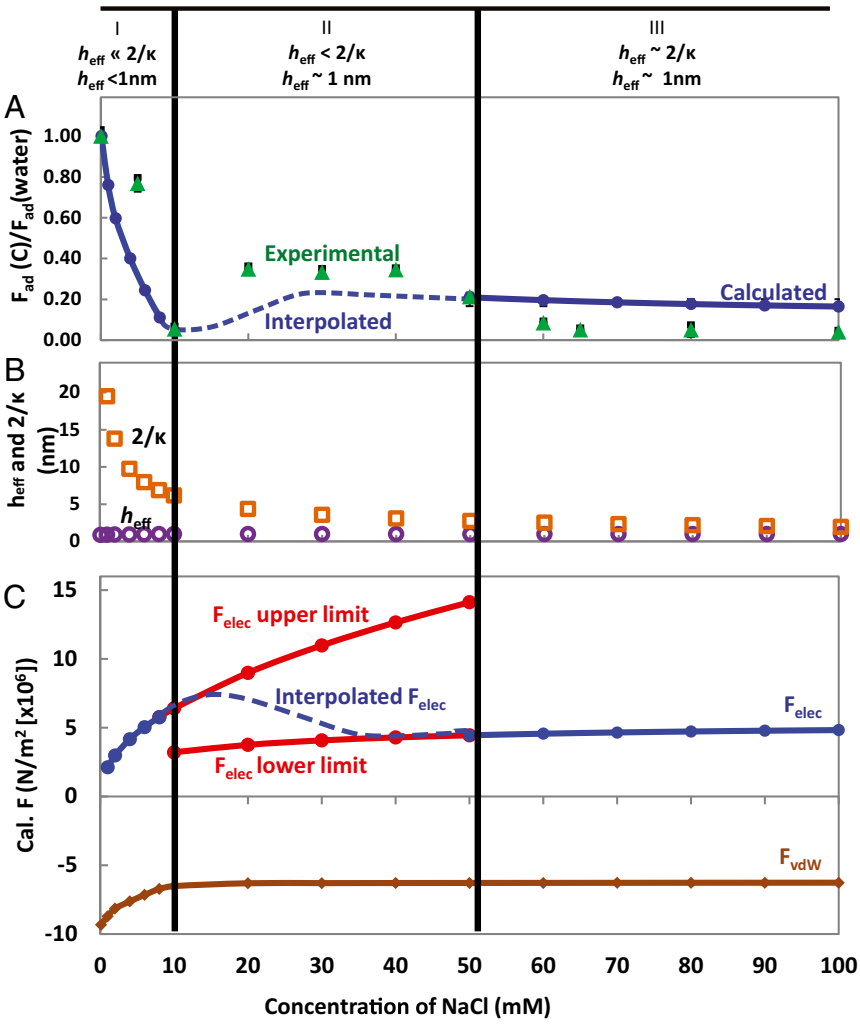

Fig. 4. Dependence of F_{ad} on NaCl concentration. (*A*) Experimental and calculated values of F_{ad} vs. C_{NaCl}. (*B*) Three regions of C_{NaCl} defined by the ratio of the estimated separation (h_{eff}) to the calculated value of 2/κ. (*C*) Calculated (solid curve) and extrapolated (dashed red curves) or interpolated (dashed blue curve) values of F_{elec} and F_{vdW} vs. C_{NaCl} based on DLVO theory modified to include the charge-regulating nature of the mica surface.

increasing T due to the larger amplitude of the thermal fluctuations away from the minimum of the bound state (24).

We now demonstrate that many of the aforementioned features can be explained with a model that considers the effects of molecular details, namely the presence of strongly adsorbed hydration layers, the number density of ionizable surface groups, and the anisotropy of the crystal lattice, on the long-range van der Waals (F_{vdW}) and electrostatic (F_{elec}) forces.

To interpret the observed behavior of F_{ad}, we first need to estimate a tip–substrate separation in the solvent-separated regime. This separation was estimated via a balance in forces from the intervening solvent structures and the compression. Our rationale for estimating an effective separation (h_{eff}) is that the AFM cantilever cannot exert a sufficient pressure to desolvate the ions (i.e., penetrate nearby hydration layers), and thus leaves the adsorbed hydrated ions between the tip and substrate intact (see *SI Appendix* for details). This estimate is consistent with the dependence of pressure on mica–mica separation determined in previous SFA experiments (16). The hydrated ions lead to h_{eff} of ~2× the hydrated ion diameter (see *SI Appendix*, Fig. S4 for details), that we predict to be ~0.7 to ~1 nm for C_{NaCl} between 0 and 10 mM (Fig. 4*B*, region I) and ~1 nm for C_{NaCl} >10 mM (Fig. 4*B*, regions II and III). As a result, whereas the hydration layer plays a critical role in determining h_{eff}, F_{ad} does not include a force associated with hydration layers; F_{ad} can be interpreted as a net attractive force at h_{eff} that is a function of the intervening solvent structure.

Next, we consider the charge-regulating nature of the mica surface by replacing the fixed surface charge/potential commonly used in a typical Derjaguin–Landau–Verwey–Overbeek (DLVO) theory (25) with the number density of ionizable groups on mica to obtain a more realistic prediction of F_{elec} (25) (see *SI Appendix*, Eq. **S3**). Following the model of Ninham and Parsegian (25), F_{elec} can be approximated in two asymptotic limits, $h_{eff} << O(2/\kappa)$ for C_{NaCl} <10 mM (Fig. 4*C*, solid blue line, region I) and $h_{eff} \sim O(2/\kappa)$ for C_{NaCl} >50 mM (Fig. 4*C*, solid blue line, region III), where κ is the inverse Debye length varying with C_{NaCl} (Fig. 4*B*) (see *SI Appendix* for details). In the intermediate region II, these expressions provide estimates of the upper and lower limits (red lines in Fig. 4*C*). The results predict that F_{elec} is always repulsive and increases steeply with increasing C_{NaCl} in region I, but is fairly constant in region III. Interpolation across region II leads to the prediction that F_{elec} exhibits a maximum and a minimum in the range of 10–50 mM NaCl, which is where the secondary maximum in F_{ad} is observed.

In contrast, F_{vdW}, which can be approximated by $F_{vdW} = -A/(6\pi h^3)$, where A is the frequency-dependent Hamaker function for the mica–water–mica system, is always attractive and nearly constant over the entire range of C_{NaCl} (Fig. 4*C*, solid brown line) (see *SI Appendix* for details). Note that the $O(1)$ nm effective separation can be used to justify Hamaker's approach as a reasonable approximation without considering details of retardation (26) and interatomic spacing (27), although A can be significantly influenced by the different dielectric response of

hydration layers (15) (see *SI Appendix* for details). The resulting prediction for electrolyte dependence of the total long-range adhesion force, $F_{ad} = F_{elec} + F_{vdW}$, is in good agreement with measured values for $0 \le C_{NaCl} \le 100$ mM (Fig. 4*A*). F_{ad} is always attractive; it drops sharply from a maximum value at $C_{NaCl} = 0$ to a minimum near $F_{ad} = 0$ for $C_{NaCl} \sim 10$ mM, reaches a small secondary maximum near $C_{NaCl} \sim 30$ mM, and drops gradually at higher NaCl concentrations. The detailed sensitivity of our fit in Fig. 4*A* to different h_{eff} (*SI Appendix*, Fig. S7) further demonstrates the predicted h_{eff} (i.e., ~1 nm) is indeed reasonable.

Our formulation of F_{ad} also predicts the observed trend with electrolyte valence (Fig. 3*A*). At 100 mM, all salt solutions satisfy $h_{eff} \sim O(2/\kappa)$. In this regime (III), the electrostatic repulsion is the smallest in pure water and the resulting F_{elec} for monovalent ions is 4× that for the divalent ions (*SI Appendix*, Fig. S6 and Eqs. **S5** and **S10**). In contrast, the variation in F_{vdW} is only ~40% (*SI Appendix*, Eqs. **S6** and **S7** and Fig. S6); thus F_{ad} is greatest in water and smallest for the monovalent ions (Fig. 3*A*). Due to the smaller radius of Mg^{2+} than Ca^{2+}, the strongly hydrated Mg^{2+} ions have weaker interactions with mica and can be more easily expelled from the surface (28), leading to lower surface ion density, smaller F_{elec}, and greater F_{ad}. Moreover, Monte Carlo simulations predict that Mg^{2+} and Ca^{2+} are adsorbed above tetrahedral sites of mica at distances of 3.45 and 3.99 Å, respectively (29, 30), resulting in a Mg^{2+} separation h_{eff} less than that of Ca^{2+}. Similarly, we predict F_{ad} for Na^+ should exceed that for K^+. (See *SI Appendix* for estimated separations and F_{ad} calculation for various ion solutions.)

The validity of the physical picture presented above is reinforced by the resulting prediction of the dependence of F_{ad} on T. The formulation of the forces suggests that a change in temperature influences F_{elec} and F_{vdW} in a complex and correlated fashion: (*i*) A varies linearly with T (26), (*ii*) the dielectric constant of water drops by nearly 20% between 5 and 45 °C (31), (*iii*) κ is a function of T, and (*iv*) the osmotic pressure is linearly proportional to T (see *SI Appendix* for details). Considering such changes, the predicted dependence of F_{ad} on T exhibits the trends observed experimentally (Fig. 3*B*), except for the unique behavior at $C_{NaCl} = 100$ mM (Fig. 3*B*). This phenomenon occurs because increasing T influences the hydration of ions, more easily disrupting the ion hydration and leading to a decreased h_{eff} (see *SI Appendix* for details). However, at $C_{NaCl} = 100$ mM, the calculations indicate that the interaction forces are highly sensitive to a choice of h_{eff} (*SI Appendix*, Fig. S8); implementing a mere 0.015-nm variation in h_{eff} from 0.95 to 0.935 nm results in a qualitatively similar trend to that seen experimentally (Fig. 3*B*; see *SI Appendix* for details).

Another important consequence of h_{eff} being $O(1)$ nm is that F_{vdW} is responsible for the observed orientation dependence (Fig. 2*A*), because F_{elec} is isotropic at such separations even in the presence of a molecular representation of the surface (see *SI Appendix* for details). However, for a biaxial crystal like mica, the molecular structure of the lattice is imprinted upon the frequency-dependent dielectric function and thus gives rise to an orientation dependence of the Hamaker constant A—now a tensor—that reflects the symmetry of the crystal (32). Based on the Lifshitz theory at zero wave-number limit (i.e., $\mathbf{k} \to 0$), the angular dependence of A is qualitatively described by $A = A_0 + A_1(1 + 2\cos^2\theta)$, where θ is the in-plane mismatch angle between crystal surfaces (i.e., principal optical axes) and A_0 and A_1 denote nonangular and angular coefficients. These coefficients are complicated functions of the dielectric properties (ε) of mica (tensorial) and water (scalar) (Fig. 2*D*) (26). Although strictly monoclinic, the structure of mica exhibits a small distortion from hexagonal symmetry (Fig. 2 *B* and *C*). This symmetry constrains mica to be nearly optically identical with every 60° rotation, implying that the angular factor should become $1 + 2\cos^2(3\theta)$. Thus, this simple analysis of the angular factor in A should provide a qualitative understanding of the observed 60° periodicity of F_{ad}. Assuming $\partial h_{eff}/\partial\theta = 0$, F_{max}/F_{min} is predicted to exhibit maxima at $\theta = 0° \pm n\cdot 60°$, where n is an integer, and minima at $\theta = 30° \pm n\cdot 60°$. For $\mathbf{k} \to 0$, our theory predicts that the magnitude of the variation in F_{max}/F_{min} (1.04) is much less than the observed factor of 2 (see *SI Appendix* for details). We leave open the possibility that h_{eff} may vary due to the variation in adhesion force at different mismatch angles. Specifically, based on our calculations, a 10–20% variation in h_{eff} (from 1 nm) would be all that is required to change F_{ad} by a factor of 1.4–2, respectively, in water. Moreover, the observed periodicity (Fig. 2*A*) diverges from a simple sixfold sinusoidal symmetry. Whereas the latter can be understood from the deviations of the mica lattice—which is actually monoclinic—from pure hexagonal symmetry, this finding suggests that consideration of both the wave-vector dependence and nonlocal dielectric response is required to quantitatively predict the trends in F_{max}/F_{min} with changes in relative orientation, as suggested in a previous work with graphite surfaces (33). Our calculations based on the aforementioned tensorial form and a naive extension of the isotropic Lorentzian formula for the frequency-dependent scalar dielectric property of mica provide support for the need of a rigorous treatment of the dielectric tensor of mica (see the discussion in *SI Appendix*).

Discussion and Conclusions

The findings presented here suggest that, in the absence of attractive dispersion forces, only the repulsive interactions of electrostatics and hydration forces would be present. Hence, it is the dispersion force that is responsible for nanocrystals retaining their proximity to one another for sufficient time to allow the (de)hydration barriers to be overcome through fluctuations of solvent layers.

An important aspect of this study is to include some of the important molecular granularity present in the solution through its response to the mica surface to calculate the long-range interactions needed to predict the observed trends in adhesion force with temperature and electrolyte type and concentration. However, a better molecular description that includes, for example, correct ion distributions as a function of separation and concentration, and nonlocal dielectric response will be necessary to obtain a quantitative prediction. Moreover, whereas obtaining a purely molecular picture through molecular simulations would be desirable, the potentials available for such simulations typically use cutoffs for the molecular interaction on the order of 1 nm; thus, the ability to predict nanoparticle interactions at the large length scales relevant to this study—and thus to the solvent-separated regime—using such methods at present seem problematic (see *SI Appendix* for details).

Our use of a continuum theory modified to include molecular details also enables us to estimate the surface separation to be ~1 nm, which is consistent with estimates based on comparison of maximum pressures applied in the AFM experiments with those measured in previous SFA experiments for which surface separation is accurately known. These molecular details include the structure of the surface hydration layers and the number density of ionizable surface groups, to elucidate the subtle competition of long-range vdW and electrostatic forces. Unfortunately, neither a simple continuum theory with spatial homogeneity nor molecular simulation using isotropic pairwise-additive interactions can provide a quantitative explanation of the azimuthally resolved variation of the adhesion force between mica sheets (see *SI Appendix* for discussion). Thus, a more rigorous treatment of vdW forces arising from a spatially varying and anisotropic dielectric response in conjunction with the role of h_{eff} at different mismatch angles is needed and will be the focus of future studies.

In conclusion, taking advantage of the near-equilibrium nature of the force measurements ($F_{ad} \sim F_{eq}$), the present study shows that F_{eq}—and hence the equilibrium binding energy—between mica surfaces in the solvent-separated regime has an ~60° periodicity related to crystal structure and depends strongly on electrolyte type, concentration, and temperature. The nonmonotonic

variation of F_{ad} with electrolyte concentration indicates the magnitude of F_{ad} is determined by competing forces. Analysis shows these features are all consistent with an attractive interaction induced by vdW forces that is indeed competing with electrostatic and hydration forces. Such balance is predicted to be very sensitive to the short-range surface hydration structure, which can be controlled via electrolyte type, concentration, and temperature, leading to changes in the dependence of force on separation and consequent variations in h_{eff}. Our findings imply that a simple model system, such as the (001) face of mica, exhibits the complexities germane to a quantitative understanding of OA of nanocrystals. The analyses reported herein highlight the strong interplay between experiment and theory needed to quantify the magnitude and define the origin of the forces that drive OA, and the key theoretical findings implicate the molecular details of the solution in response to the anisotropy of the crystal in determining driving forces for assembly. The fundamental understanding arising from this study will affect phenomena beyond OA such as aggregation/disaggregation, and contraction and swelling of soil minerals in response to wetting cycles, which are largely driven by the interplay of interfacial and hydrodynamic forces.

Methods

Tip Fabrication and Force Measurements. Crystallographically oriented face-specific AFM "mica tips" with a (001) plane for a force probe were fabricated using focused ion-beam milling (Helios NanoLab 600i, FEI) and microlithography methods (see *SI Appendix* for details). A mica single crystal as substrate was mounted on the AFM substrate holder. Force measurements were performed with a commercial AFM (MFP3D or Cypher, Asylum Research). Adhesion forces (or rupture forces) were determined by a cantilever deflection and calibrated spring constant of the cantilever. The retract velocity was changed after every approach/retract cycle (keeping the approach velocity constant) to obtain a distribution of the adhesion forces at different loading rates, ranging from 2 to 150 nN/s. Approximately 25–100 measurements were taken at each loading rate, the dwell time of the tip with the substrate was 3–6 s, and an external force of a few nanonewtons was applied on the cantilever before pulling away. The geometry of the tip and substrate contact remains constant during the rotation of the substrate, and it does not influence the effect of crystal orientation on F_{ad} between mica surfaces. To investigate the orientation-dependent interactions, a rotation stage was mounted on the substrate holder. The substrate was rotated from 0° to 360° while the orientation of the AFM cantilever tip was fixed. Mismatch angle was recorded for one set of experiments (see *SI Appendix* for details). The spring constants of all cantilevers were calibrated by the thermal fluctuation method. The measurements presented here were performed with two different cantilevers with spring constants of ~50 and ~700 pN/nm. All measurements were performed at room temperature unless noted. All chemicals were purchased from Sigma Aldrich, unless noted. F_{ad} was determined at a pH of 5.6 ± 0.1 for a range of tip retraction rates, NaCl concentrations (0–100 mM), electrolyte species (NaCl, KCl, $MgCl_2$, and $CaCl_2$), relative tip–substrate rotation angles (0–360°), and temperatures (15–45 °C). The mismatch angle was kept constant during the measurement while changing the salt concentration, temperature, and ionic species. For more detailed information please see *SI Appendix*.

ACKNOWLEDGMENTS. We thank Sebastien Kerisit for discussions of molecular dynamics simulation. DFS measurements were supported by the US Department of Energy (DOE), Office of Basic Energy Sciences (BES), Division of Materials Science and Engineering (DMSE) through Early Career Research Program Award 67037. Theoretical analysis was supported by the DOE BES DMSE. The development of approaches to both nanocrystal tip fabrication and force measurement were supported by the National Science Foundation under Grant DMR-1312697, and development of the theoretical approach to analyzing forces was supported by the Materials Synthesis and Simulations across Scales Initiative, a Laboratory Directed Research and Development Program at Pacific Northwest National Laboratory (PNNL). Data processing was supported by the Young Talent Support Plan of Xi'an Jiaotong University and the Education Program for Talented Students of Xi'an Jiaotong University. Tip fabrication was performed in the Environmental and Molecular Sciences Laboratory, a DOE Office of Science User Facility sponsored by the Office of Biological and Environmental Research and located at PNNL. PNNL is a multiprogram national laboratory operated for DOE by Battelle under Contract DE-AC05-76RL01830.

1. De Yoreo JJ, et al. (2015) Crystal growth. Crystallization by particle attachment in synthetic, biogenic, and geologic environments. *Science* 349:aaa6760.
2. Dey A, et al. (2010) The role of prenucleation clusters in surface-induced calcium phosphate crystallization. *Nat Mater* 9:1010–1014.
3. Demichelis R, Raiteri P, Gale JD, Quigley D, Gebauer D (2011) Stable prenucleation mineral clusters are liquid-like ionic polymers. *Nat Commun* 2:590.
4. Penn RL, Banfield JF (1998) Imperfect oriented attachment: Dislocation generation in defect-free nanocrystals. *Science* 281:969–971.
5. Li D, et al. (2012) Direction-specific interactions control crystal growth by oriented attachment. *Science* 336:1014–1018.
6. Li D, et al. (2013) Growth mechanism of highly branched titanium dioxide nanowires via oriented attachment. *Cryst Growth Des* 13:422–428.
7. Fiore A, et al. (2009) Tetrapod-shaped colloidal nanocrystals of II-VI semiconductors prepared by seeded growth. *J Am Chem Soc* 131:2274–2282.
8. Boneschanscher MP, et al. (2014) Long-range orientation and atomic attachment of nanocrystals in 2D honeycomb superlattices. *Science* 344:1377–1380.
9. Franchini IR, et al. (2010) Phototransport in networks of tetrapod-shaped colloidal semiconductor nanocrystals. *Nanoscale* 2:2171–2179.
10. Liao H-G, Cui L, Whitelam S, Zheng H (2012) Real-time imaging of Pt_3Fe nanorod growth in solution. *Science* 336:1011–1014.
11. Cho K-S, Talapin DV, Gaschler W, Murray CB (2005) Designing PbSe nanowires and nanorings through oriented attachment of nanoparticles. *J Am Chem Soc* 127:7140–7147.
12. Yuwono VM, Burrows ND, Soltis JA, Penn RL (2010) Oriented aggregation: Formation and transformation of mesocrystal intermediates revealed. *J Am Chem Soc* 132:2163–2165.
13. McGuiggan PM, Israelachvili JN (1990) Adhesion and short-range forces between surfaces. Part II: Effects of surface lattice mismatch. *J Mater Res* 5:2232–2243.
14. Finot E, Lesniewska E, Mutin J-C, Goudonnet J-P (2000) Investigations of surface forces between gypsum microcrystals in air using atomic force microscopy. *Langmuir* 16:4237–4244.
15. Chun J, Mundy CJ, Schenter GK (2015) The role of solvent heterogeneity in determining the dispersion interaction between nanoassemblies. *J Phys Chem B* 119:5873–5881.
16. Kilpatrick JI, Loh S-H, Jarvis SP (2013) Directly probing the effects of ions on hydration forces at interfaces. *J Am Chem Soc* 135:2628–2634.
17. Pashley RM (1981) DLVO and hydration forces between mica surfaces in Li+, Na+, K+, and Cs+ electrolyte solutions: A correlation of double-layer and hydration forces with surface cation exchange properties. *J Colloid Interface Sci* 83:531–546.
18. Israelachvili JN, McGuiggan PM (1990) Adhesion and short-range forces between surfaces. Part I: New apparatus for surface force measurements. *J Mater Res* 5:2223–2231.
19. Meleshyn A (2008) Aqueous solution structure at the cleaved mica Surface: Influence of K+, H3O+, and Cs+ adsorption. *J Phys Chem C* 112:20018–20026.
20. Cheng L, Fenter P, Nagy KL, Schlegel ML, Sturchio NC (2001) Molecular-scale density oscillations in water adjacent to a mica surface. *Phys Rev Lett* 87:156103.
21. Leng Y (2012) Hydration force between mica surfaces in aqueous KCl electrolyte solution. *Langmuir* 28:5339–5349.
22. Friddle RW, Noy A, De Yoreo JJ (2012) Interpreting the widespread nonlinear force spectra of intermolecular bonds. *Proc Natl Acad Sci USA* 109:13573–13578.
23. Butt H-J (1991) Measuring electrostatic, van der Waals, and hydration forces in electrolyte solutions with an atomic force microscope. *Biophys J* 60:1438–1444.
24. Noy A, Zepeda S, Orme CA, Yeh Y, De Yoreo JJ (2003) Entropic barriers in nanoscale adhesion studied by variable temperature chemical force microscopy. *J Am Chem Soc* 125:1356–1362.
25. Ninham BW, Parsegian VA (1971) Electrostatic potential between surfaces bearing ionizable groups in ionic equilibrium with physiologic saline solution. *J Theor Biol* 31:405–428.
26. Parsegian VA (2006) *Van der Waals Forces: A Handbook for Biologists, Chemists, Engineers, and Physicists* (Cambridge Univ Press, Cambridge, UK), p 45.
27. White LR (2010) van der Waals interaction energy and disjoining pressure at small separation. *J Colloid Interface Sci* 343:338–343.
28. Pashley RM, Israelachvili JN (1984) DLVO and hydration forces between mica surfaces in Mg2+, Ca2+, Sr2+, and Ba2+ chloride solutions. *J Colloid Interface Sci* 97:446–455.
29. Meleshyn A (2009) Potential of mean force for Mg2+ at the cleaved mica–water interface. *J Phys Chem C* 113:12946–12949.
30. Meleshyn A (2009) Potential of mean force for Ca2+ at the cleaved mica–water interface. *J Phys Chem C* 113:17604–17607.
31. Owen BB, Miller RC, Milner CE, Cogan HL (1961) The dielectric constant of water as a function of temperature and pressure. *J Phys Chem* 65:2065–2070.
32. Röthel C, et al. (2015) Complex behavior of caffeine crystallites on muscovite mica surfaces. *Cryst Growth Des* 15:4563–4570.
33. Li J-L, et al. (2005) Use of dielectric functions in the theory of dispersion forces. *Phys Rev B* 71:235412.